Journal of
Mechanics of
Materials and Structures

DEEP PENETRATION AND LIQUID INJECTION INTO ADIPOSE TISSUE

Kerstyn Comley and Norman Fleck

■
■■msp

DEEP PENETRATION AND LIQUID INJECTION INTO ADIPOSE TISSUE

KERSTYN COMLEY AND NORMAN FLECK

The subcutaneous injection of porcine adipose tissue by a hypodermic needle involves two stages: tissue penetration followed by the delivery of liquid into the tissue. The force required to penetrate adipose tissue by a series of conically tipped and flat-bottomed circular punches has been measured. Scanning electron microscopy and light microscopy are used to observe the mechanism of crack formation during penetration. The experiments reveal that penetration by either a flat bottomed or 45° conically tipped punch involves the formation of a mode II ring crack. The predicted penetration pressure according to the Shergold–Fleck model (Proc. R. Soc. Lond. A **460** (2004), 3037–3058) is in good agreement with the measured pressure on the punch. The subsequent delivery of liquid into adipose tissue by the hypodermic needle has also been examined: the injection pressure for phosphate buffered saline has been measured for a range of flow rates. X-ray images of the injected liquid suggest that micro-cracks are formed by the fluid pressure within the tissue and this leads to an increase in permeability. A seepage model is developed, based on the Darcy flow law, to relate the volumetric flow rate to the injection delivery pressure. Finally, a model of hydraulic fracture is used to assess the toughness associated with the formation of the micro-cracks during injection.

1. Introduction

A wide range of medical devices exist for the injection of liquid-based drugs into the subcutaneous layer of adipose tissue. These include a hypodermic needle and a needle-free syringe. Injection involves two stages: (i) a needle or liquid jet penetrates the tissue to a desired depth (intradermal, subcutaneous, intramuscular and so on); and (ii) the liquid drug is delivered from the syringe into the tissue. Needle-free devices achieve control of tissue penetration and liquid delivery through control of the pressure versus time characteristic of the jet. For example, when subcutaneous injection occurs by a needle-free device, the dermal and subcutaneous layers are first penetrated by a high pressure jet (static head of order 25 MPa for 5 ms). Subsequent delivery of the bulk of the liquid into the subcutaneous layer follows at a lower jet pressure (static head of approximately 5 MPa) and typically takes 100 ms [Shergold et al. 2006].

Consider first the penetration stage. Shergold and Fleck [2004] have recently developed two penetration models for soft solids; a model based on the formation of a planar crack and a model based on the formation of a ring-crack. They demonstrated that the force to penetrate dermis with a sharp metal punch depends upon the Young's modulus and toughness of the tissue, and upon the diameter and tip geometry of the punch. They argue that both a sharp tipped needle and a liquid jet penetrate a soft solid by the formation and opening of a planar crack, whereas penetration by a flat-bottomed punch involves the formation of a ring crack. The predicted pressure for penetration of the dermis by a liquid jet is of similar value to the pressures employed in needle-free injectors [Shergold et al. 2006]. The

Shergold-Fleck model gives the penetration pressure but no explicit information on the penetration depth. The depth of penetration achieved by high speed liquid jet injections has been measured by Baxter and Mitragotri [2005]: The depth of penetration into dermis and subcutaneous adipose tissue was a function of both the diameter and velocity of the jet.

Second, consider the liquid-delivery stage. To date, research into the mechanisms governing the delivery of liquid injected into soft tissue has been confined to an examination of the depth of the injection and the degree of dispersion of the liquid within the tissue. Differences in the dispersion behaviour of liquid injected at low and high speed may affect the rate at which a drug is absorbed and may result in the formation of different types of wound within the tissue. Cooke et al. [1980] have compared the bioavailability from a needle-free injection and from a hypodermic needle and syringe for subcutaneous and intramuscular injections of lignocane into humans. For both injection methods, the injectate was dispersed to a similar degree within the tissue. More recently, Schramm-Baxter and Mitragotri [2004] have performed liquid jet injections into human dermis and observed that the shape and dispersion of the liquid depends upon nozzle diameter and upon the jet velocity. Barry et al. [1995] have developed a poroelastic model for the seepage of a liquid into a spherical cavity, and have included the effect of the fluid pressure upon the small-strain elastic deformation of the porous medium. The relevance of this model to fluid delivery must await an experimental observation of the injection mechanism.

Scope of the paper.   The aim of the current study is to investigate the penetration and delivery of liquid into subcutaneous adipose tissue. We begin by reviewing the microstructure and mechanical properties of adipose tissue. The study is split into two parts: penetration of adipose tissue by a solid punch, and liquid injection by hypodermic syringe. In Section 2, penetration tests by conically tipped and flat-bottom punches are reported, and scanning electron microscopy, light microscopy are used to reveal the mechanisms of penetration. The results are compared with existing models in Section 3. The response of adipose tissue to hypodermic injection is described in Section 4. X-ray techniques are used to reveal the mechanisms of liquid delivery and are combined with the results from the injection tests to motivate a seepage model in Section 5. Concluding remarks are stated in Section 6.

Review of the microstructure and mechanical properties of adipose tissue.   Subcutaneous adipose tissue is a connective tissue comprising lipid-filled cells called *adipocytes* and resides directly under the dermal layer of human skin. The lipid is a triacylglyceride of molecular weight on the order of $900\,\text{g mol}^{-1}$ and viscosity of $40\,\text{mPa s}$ at $37°$ C [Comley and Fleck 2010a]. The adipocytes are of diameter $80\,\mu\text{m}$ and are supported by two interpenetrating collagen-based structures: (i) a *reinforced basement membrane* in the form of a collagen mesh, containing primarily type I and IV collagen, surrounds each cell, and (ii) a type I collagen fibre network, termed the *interlobular septa* [Björntorp and Martinsson 1966; Nakajima et al. 1998]. The reinforced basement membrane resembles a closed cell foam with a unit cell dimension of $80\,\mu\text{m}$ and walls of thickness $2\,\mu\text{m}$. In contrast, the interlobular septa take the form of an open cell foam with cell edge length $1\,\text{mm}$ and a cell wall thickness of $10\,\mu\text{m}$ [Comley and Fleck 2010a]. The macroscopic stiffness and toughness derive primarily from the reinforced basement membrane.

Additional structures such as blood vessels exist within the tissue, but have negligible influence on the overall mechanical properties. The intervening space is filled with *ground substance*. Overall, 60–80% (by mass) of adipose tissue is lipid, 5–30% is water and the remaining 2–3% is protein [Greenwood and Johnson 1983]. The large liquid content enforces material incompressibility [Samani et al. 2003].

Histology of adipose tissue suggests that it is approximately isotropic in structure and is thereby isotropic in mechanical properties, to a first approximation [Samani et al. 2003; Comley and Fleck 2010a].

Uniaxial compression tests of adipose tissue suggest that at low strain rates (on the order of 10^{-3} s^{-1}) the tissue has a Young's modulus of approximately $E = 1$ kPa, whereas at strain rates of order 1000 s^{-1} the modulus increases by more than three orders of magnitude to $E = 3$ MPa [Miller-Young et al. 2002; Nightingale et al. 2003; Gefen and Haberman 2007; Comley and Fleck 2009]. Comley and Fleck [2011] demonstrates that the stress versus strain behaviour of adipose tissue can be adequately described by a one term Ogden strain energy density function [1972] with a shear modulus $\mu = E/3$ and strain hardening exponent $\alpha = 20$ of the form

$$\phi = \frac{2\mu}{\alpha^2}(\lambda_1^\alpha + \lambda_2^\alpha + \lambda_3^\alpha - 3) \tag{1}$$

Here, ϕ is the strain energy density per undeformed unit volume and λ_i are the three principal stretch ratios.

2. Penetration tests using a solid punch

Test method. Deep penetration tests were performed on samples of adipose tissue using circular, cylindrical punches of conical and flat bottomed headshape. Fresh porcine adipose tissue from the jowl of a pig was obtained (Dalehead Foods, Linton, Cambridgeshire, UK), cut into rectilinear blocks of approximate dimension 30 mm × 30 mm by 10 mm thick and stored in phosphate buffered saline (PBS) prior to testing. Testing always commenced within four hours of slaughter.

Cylindrical steel punches of diameter in the range $2R = 0.4$ mm to $2R = 3.9$ mm were machined with either a flat bottom or a conical tip of semi-included apex angle 45°. The punches were then mounted on the cross-head of a screw-driven tensile test machine. A block of adipose tissue was placed on a PMMA plate (thickness 10 mm), placed in turn on the test-machine platen. The penetration force F versus displacement u was measured at selected displacement rates in the range 0.05 mm s^{-1} to 10 mm s^{-1}. The cross-head was displaced until the punch made contact with the PMMA plate. Three tests were performed for each configuration of punch and displacement speed. Measurements of the friction force between the side wall of the punch and the tissue following full penetration of the specimen were additionally made as follows. A specimen was placed on a PMMA block containing a through hole of diameter three times that of the punch. The centre-line of the hole was in line with that of the punch and the punch was depressed until its tip penetrated the lower surface of the tissue and passed into the hole in the support block. Continued pushing of the punch through the tissue required a friction force F_{fric}.

Force versus displacement results. A representative set of F versus u results for punches with a diameter $2R = 0.6$ mm is shown in Figure 1. The response is qualitatively the same for the flat-tipped punch and the punch with the 45° conical tip. For both headshapes, the force increases steadily with punch displacement until the front surface of the tissue is penetrated. After penetration of the front face, the punch enters the tissue and the force oscillates about a mean (plateau) value F_p. These oscillations in force are associated with the propagation of the crack ahead of the punch tip. Similar profiles of force versus displacement were seen for all punch diameters tested, according to their tip type. Displacement rate was not found to have a significant effect on the measured force. These additional curves are omitted for the sake of brevity.
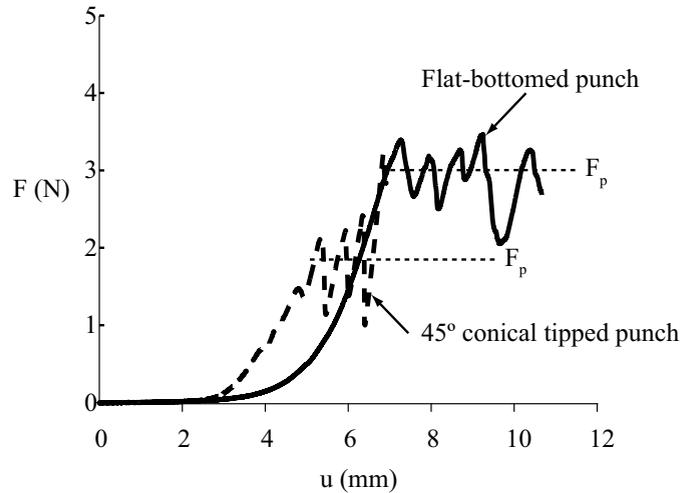
Figure 1. Force F versus displacement u for the penetration of porcine adipose tissue with 0.6 mm diameter metal punches with either a flat-bottom (solid line) or a 45° conical tip (dashed line). The displacement rate was 0.1 mm s^{-1}.

The frictional force F_{fric} between the shaft of the punch and the tissue, following full penetration of the specimen, was less than 5% of the average plateau force F_p. This is consistent with the observation that the penetration force oscillates about a mean value F_p, with no observable rise in F_p due to frictional effects.
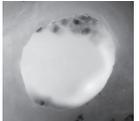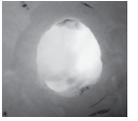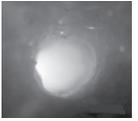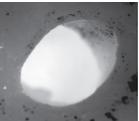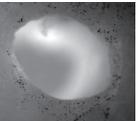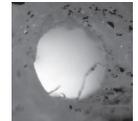
Observations of hole formation. Observations of the hole formation in the tissue were made as follows. Upon removal of the punch the surfaces of a selection of samples were examined with an optical microscope. A separate set of samples were fixed in glutaraldehyde, sectioned along the diametral plane of the hole and prepared for viewing in a scanning electron microscope (SEM). See [Comley and Fleck 2010a] for full details of sample preparation.

The hole generated by each punch was observed by both light microscopy and a scanning electron microscope (SEM). The residual hole at the front face of the tissue is shown in Figure 2, for a range of punch diameters and headshapes. In all cases, the residual hole was almost circular in shape and of diameter about 20% less that that of the punch.
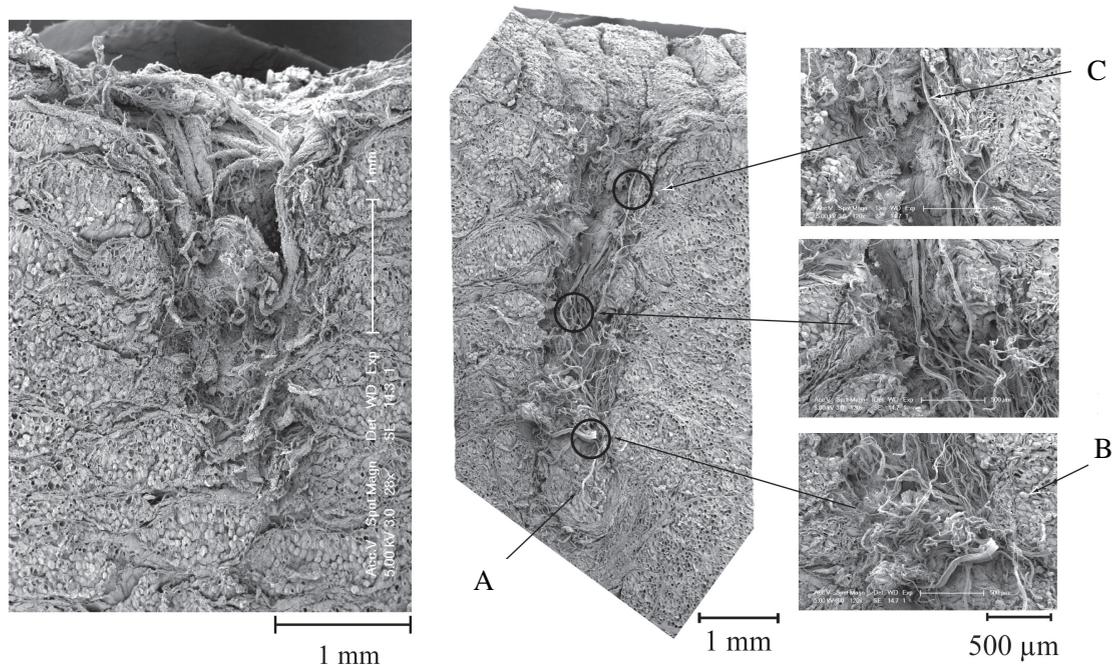
SEM images of the fracture surface following penetration are shown in Figure 3 for both the flat-bottomed punch and the 45° conical tipped punch. Adipocyte cells have ruptured and septa fibres have pulled out and torn, as labelled in the figure. Reinforced membrane and septa fibres are compacted at the bottom of each hole.

3. Discussion of the penetration behaviour

The nominal penetration pressure p is now examined for the full range of punch diameters and headshapes that have been tested. Penetration pressure is a useful quantity for comparison with the penetration models of [Shergold and Fleck 2004] and for comparison with the pressures required for liquid injection. It is

Punch diameter

Punch tip	3.9 mm	2.4 mm	0.6 mm
Flat	1 mm	1 mm	0.5 mm
45° Conical	1 mm	1 mm	0.5 mm

Figure 2. Images of the puncture site at the tissue surface following puncture by a range of metal punches of varying headshape at $0.1\,\mathrm{mm\,s^{-1}}$.

Figure 3. SEM images of the fracture surface of adipose tissue punctured by two punches of diameter 2.4 mm and tip geometry. Left: 45° conical tipped. Middle and right: flat-bottomed (A: compacted interlobular septa and reinforced basement membrane; B: interlobular septa fibres; C: reinforced basement membrane surrounding an adipocyte.
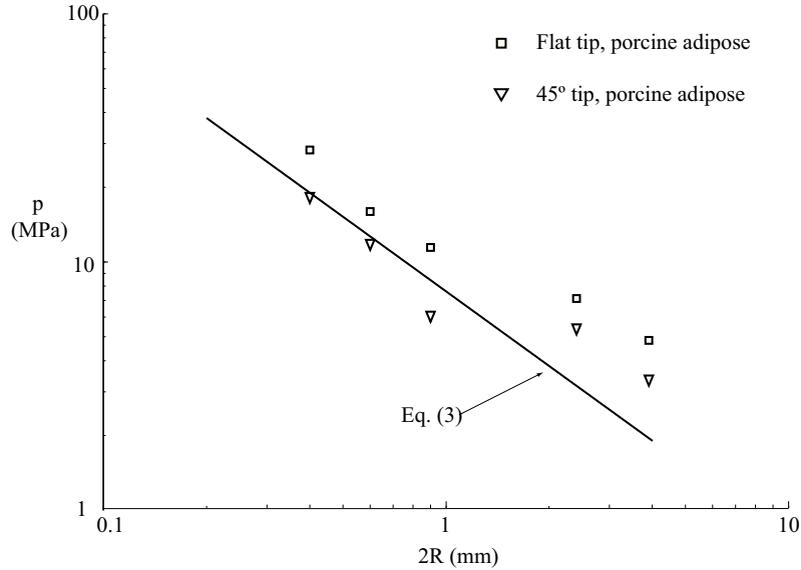
Figure 4. Comparison of the average pressure p required to penetrate adipose tissue with a range of solid punches of varying headshape. A prediction is shown for the pressure required to puncture adipose tissue with a flat tipped punch calculated from (3). The following parameter values were used in the calculations: $J_C = 4.1\,\text{kJ}\,\text{m}^{-2}$, $b/R = 0.5$, $a/R = 0.8$, $\mu = E/3 = 0.3\,\text{kPa}$.
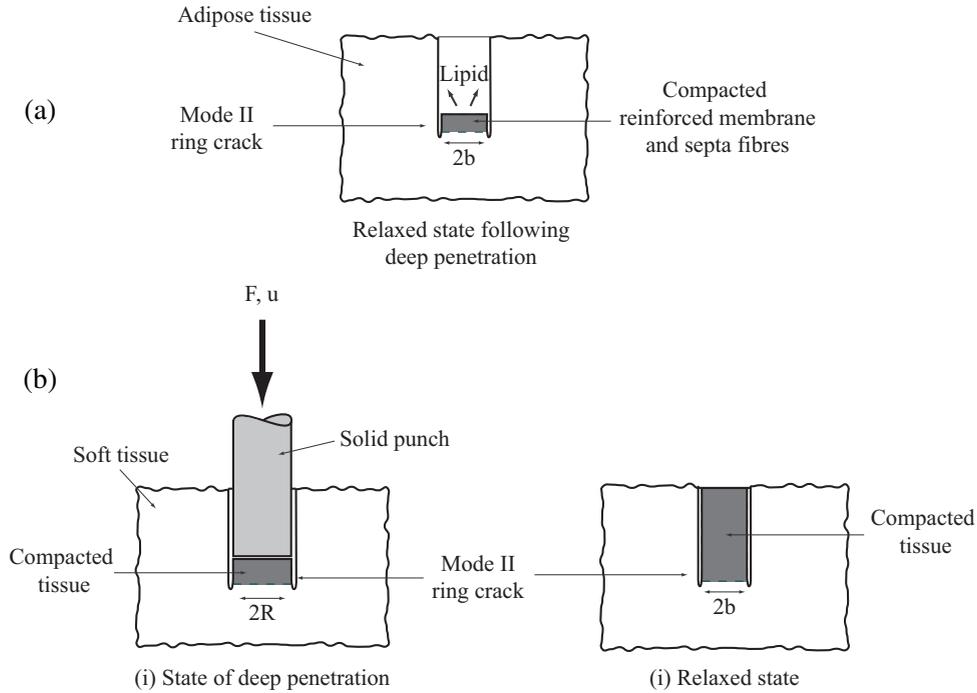
defined by

$$p = \frac{F_p}{\pi R^2} \tag{2}$$

in terms of punch force F_p and punch radius R. For each headshape, the average penetration pressure p (taken from the pooled set of pressure results across all the displacement rates tested) is plotted as a function of punch diameter $2R$ (see Figure 4). For a given punch diameter $2R$ the penetration pressure for the flat-bottomed punch exceeds that for the 45° tipped punch.

We note in passing that the pressure to penetrate adipose tissue with a flat-bottomed punch is half the magnitude of the pressure to penetrate dermal tissue (a related collagen based connective tissue) with a similar punch. Pressures of 60 MPa were recorded in [Shergold and Fleck 2005] during tests *in vivo* on human dermis with a 0.3 mm diameter flat-bottomed punch. This compares to 30 MPa needed to penetrate adipose with a 0.4 mm diameter flat-tipped punch.

Shergold and Fleck [2004] have developed two models for the deep penetration of a soft solids (see Section 1). In order to select the appropriate Shergold-Fleck penetration model for comparison with the measured penetration pressures it is necessary to determine the mode of hole formation, during penetration. The light microscopy and SEM images of Figures 2 and 3 suggest that both the flat-bottomed and the 45° conical tipped punches compact a circular cylindrical slug of tissue beneath the punch (see Figures 3 and 5a). This indicates that a mode II ring crack is generated in adipose tissue during penetration by either a flat-bottomed or 45° conical tipped punch. The characteristics of the puncture force response, shown in Figure 1, are consistent with force response observed in [Shergold et al. 2006] for punches that

(a) Adipose tissue

Lipid

Mode II
ring crack

Compacted
reinforced membrane
and septa fibres

2b

Relaxed state following
deep penetration

(b)

F, u

Soft tissue

Solid punch

Compacted
tissue

Mode II
ring crack

Compacted
tissue

2R

2b

(i) State of deep penetration   (i) Relaxed state

Figure 5. Sketches of (a) the hole formation in adipose tissue following deep penetration
by a flat tipped or 45° conical tipped punch, and (b) the hole formation of the Shergold-
Fleck ring-crack model.

generate ring cracks. Also the lack of a frictional component to the measured penetration force provides
further evidence of ring-cracking. It now remains to briefly review the model and then compare the
predictions from the model with the observed penetration pressures reported in Figure 4.

Application of the Shergold-Fleck ring-cracking model. Shergold and Fleck [2004] observed that a flat-
bottomed punch generated a mode II ring crack below the punch. Their model is sketched in Figure 5b.
They predicted that the pressure p_f scaled with the toughness J_C and shear modulus μ according to

$$\frac{p_F}{\mu} = \left[1 - \left(\frac{b}{R}\right)^2\right]^{-1} \left[\frac{2b}{R}\frac{J_C}{\mu R} + f\left(\frac{b}{R}\right)\right] \tag{3}$$

where b is the radius of the ring crack in the relaxed configuration (Figure 5b). The function $f(b/R)$ does
not exist in closed form but is defined in Equation (3.17) of [Shergold and Fleck 2004]; the details are
omitted here. The pressure given by (3) attains a minimum for a particular value of b/R and, following
that paper, we take the minimum value to be the penetration pressure for ring cracking. Upon assuming
that $J_C = 4.1\,\mathrm{kJ\,m^{-2}}$, from the trouser-tear tests of [Comley and Fleck 2010b], and taking $\mu = E/3 = 0.3\,\mathrm{kPa}$ and $\alpha = 20$ (as discussed in the introduction) we find that as $2R$ increases from 0.4 mm to
3.9 mm, b/R increases from approximately 0.48 to 0.53, whereas p_f decreases from 17 MPa to 3 MPa.
For simplicity a single value of $b/R = 0.5$ is used for the remainder of the study.

The Shergold-Fleck model is now compared to the measured data. Using the values for toughness J_C, shear modulus μ and b/R given above predictions for the penetration pressure calculated from (3) are compared to the measured data in Figure 4. The ring-cracking model is in good agreement with the experimental data for punches of diameter $2R$ less than 1 mm. The pressure to penetrate adipose tissue with punches of diameter greater than 1 mm is underestimated by the ring-cracking model. Further measurements from punches of diameter greater than 10 mm are required in order to establish whether this discrepancy is a statistical artefact or a physical effect.

Finally the prediction of $b/R = 0.5$ can be compared to the measured diameter of the holes, created by punch penetration, divided by the corresponding punch radius. Recall that the diameters of the holes were on average 80% smaller than the corresponding punch radius, suggesting an observed b/R of 0.8. The model assumes non-linear elastic behaviour whereas viscoelastic effects would lead to stress relaxation within the adipose tissue in the vicinity of the penetrator. It is unclear, however, whether viscoelastic effects are significant in these tests, as no time dependence of residual hole diameter was observed over a period of minutes following the penetration test. In a parallel study, Comley and Fleck [2009] have explored the sensitivity of uniaxial response of adipose tissue to strain rate. They found that the response is independent of strain rate in the range 10^{-4} to $1\,\mathrm{s}^{-1}$, implying that viscoelastic effects are minor over this regime.

4. Injection tests

Test methods. Measurements were made of the force to inject PBS into blocks of adipose tissue (dimension $20\,\mathrm{mm} \times 20\,\mathrm{mm} \times 10\,\mathrm{mm}$) using a hypodermic syringe. A plastic 5 ml syringe was clamped directly beneath the cross-head of a screw driven tensile test machine (see Figure 6). The syringe body was clamped at the top, above the rubber seal of the plunger, to prevent distortion of the portion of the syringe barrel containing the PBS. The syringe was fitted with either a gauge 27 hypodermic needle (internal orifice diameter $D = 0.21\,\mathrm{mm}$, needle length $L = 20\,\mathrm{mm}$) or a gauge 21 hypodermic needle (internal orifice of $D = 0.51\,\mathrm{mm}$, needle length $L = 25\,\mathrm{mm}$). The internal cross-sectional area of the
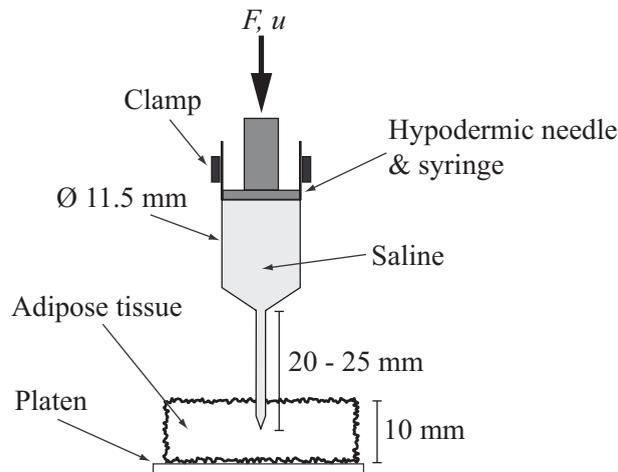
Figure 6. Experimental setup for injection tests into adipose tissue.
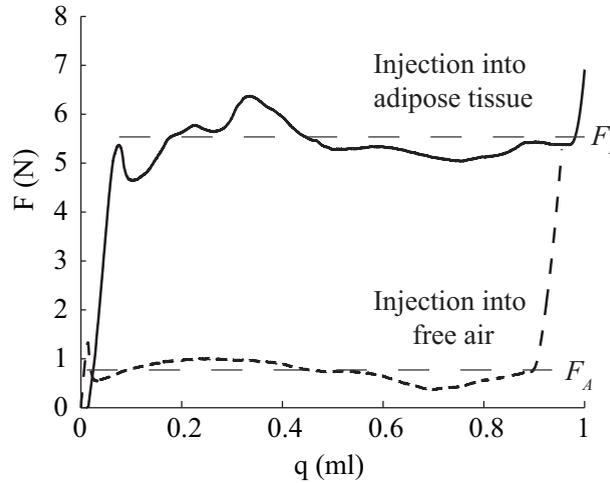
Figure 7. Force F versus the volume of saline injected q using a 0.4 mm diameter hypodermic syringe with a cross head displacement rate of $0.1 \, \mathrm{mm \, s^{-1}}$.

syringe was $A_S = 103 \, \mathrm{mm^2}$. In each injection test, the plunger was depressed into the syringe by the cross-head and the force F versus cross head displacement u were recorded in two stages, as follows:

Stage 1: The force to inject 1 ml PBS into free air was measured.

Stage 2: The syringe was re-filled with PBS. A fresh piece of adipose tissue was placed on the platen of the test-machine. The clamped syringe was manually lowered to insert the needle into the tissue to a depth of 4 mm (see Figure 6). The force to inject 1 ml PBS into the tissue was then measured.

Tests were conducted at a cross-head displacement speed in the range of $0.05 \, \mathrm{mm \, s^{-1}}$ to $1 \, \mathrm{mm \, s^{-1}}$. A fresh needle and syringe was used for each test.

Test results. Representative results for both stage 1 and stage 2 of an injection test are shown in Figure 7, for a 27 gauge needle and a cross-head displacement rate of $0.1 \, \mathrm{mm \, s^{-1}}$. Injection into air requires a level of force F_A, equal to 1 N for the data shown. In contrast, the force to inject PBS into the tissue increases with injected volume to an approximately constant level F_I, equal to 5.5 N for the data shown. The pressure to inject into adipose tissue p_D is calculated as

$$p_D = \frac{(F_I - F_A)}{A_S} \tag{4}$$

where A_S is the cross-sectional area of the syringe. The dependence of p_D upon the volumetric flow rate $\dot{q}$ is shown in Figure 8. A least squares regression reveals a linear relation between p_D and $\dot{q}$ of the form

$$p_D = c\dot{q} + p_0 \tag{5}$$

where c and p_0 are independent of the needle diameter. Values for the coefficients were found to be $c = 740 \, \mathrm{GPa \, s \, m^{-3}}$ and $p_0 = 23 \, \mathrm{kPa}$, with a measure of fit $R^2 = 0.9$. An explanation for the origins of (5) is given below.
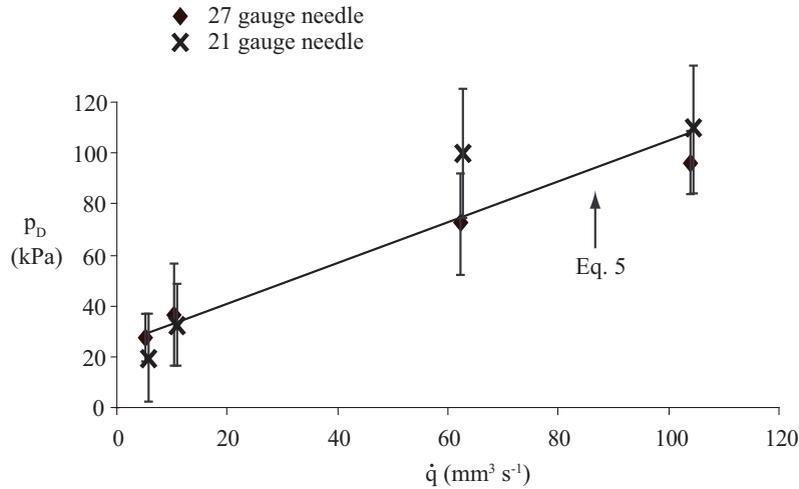
Figure 8. The mean pressure $p_d \pm$ s.d. versus volumetric flow rate $\dot{q}$ for the injection of PBS into adipose tissue using a 27 gauge needle and a 21 gauge needle. A least squares regression fit overlays the data.

X-ray imaging of injected liquid. Adipose tissue was injected with 0.5 ml of Urografin 150 (Bayer Plc, UK) radio-opaque fluid (viscosity similar to water) using a hypodermic syringe with a 21 gauge needle. Following injection the specimen was immediately placed in an x-ray inspection scanner (HMX160, X-Tech, Metris, Tring, UK) and 720 images were taken at 0.5° intervals about a 360° rotation. Image reconstruction software was used to generate a 3D representation from the 2D images.

X-ray images of the injection sites are shown in Figure 9. Examination of cross sections from the 3D reconstruction of the x-ray images show an ellipsoid shaped bolus of liquid embedded within the tissue. The injectate is distributed within micro-channels of maximum length 1 mm. The volume of the bolus is approximately 2300 mm^3. Recall that 0.5 ml Urografin fluid was injected. Consequently the average volume fraction of Urografin fluid in the overall bolus equals 0.23.

5. Discussion of injection response

The delivery pressure required to injected a liquid at low injection velocity is 10^3 times less than the pressure required for deep penetration by a solid punch. This suggests that different fracture mechanisms are involved. A seepage model for the delivery pressure and a hydraulic fracture model of the micro-cracks formed during liquid delivery are now assessed.

A model for delivery pressure. A model is now developed which describes the flow of a fluid from a spherical reservoir at the tip of the needle into micro-cracks that are created within the tissue during an injection. It is suggested that the dependence of delivery pressure p_D on volumetric flow rate $\dot{q}$ can be modelled by Darcy's law [Wang 2000]. Measurements of delivery pressure p_D are used to estimate the permeability k of the tissue during an injection, and possible mechanisms for the formation of the micro-cracks are assessed.

(i) (ii) (iii)
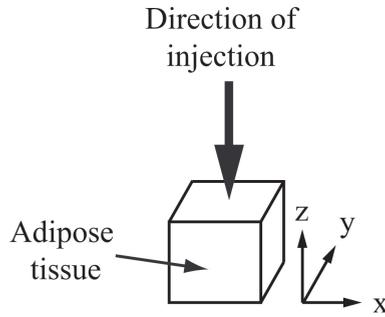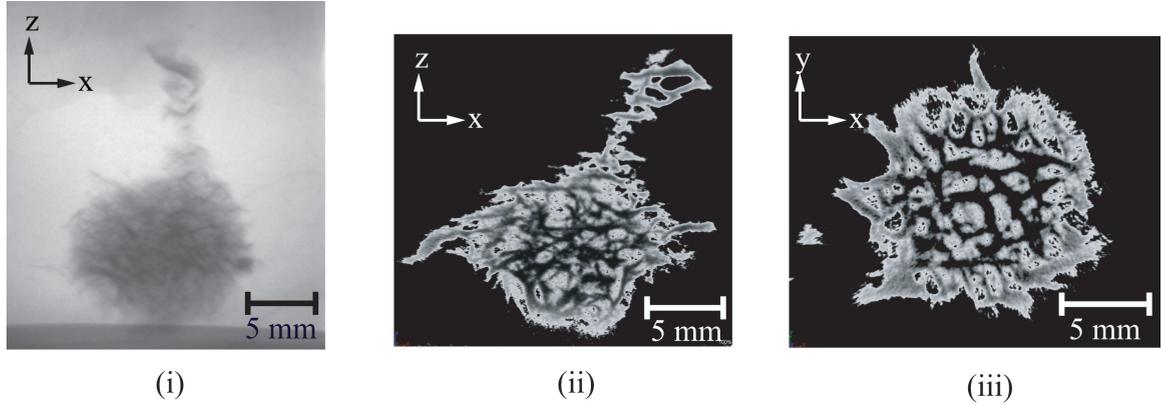
Figure 9. X-ray images of injection of 0.5 ml radio opaque dye (150 Urografin) into porcine adipose tissue by a hypodermic needle and syringe. Image (i) is a composite x-ray image. Images (ii) and (iii) are cross sections from a 3D reconstruction of 720 images taken at 0.5° around 360° of the sample.

First we examine the use of Darcy's law to model delivery pressure p_D. Darcy's law describes the nominal flow rate per unit area $\dot{u}$ as a function of the pressure gradient ∇_p and the permeability of the solid k, where

$$\dot{u} = -k\nabla_p \tag{6}$$

A model of the permeation of the injected fluid can be established as follows, see Figure 10. A fluid at a volumetric flow rate $\dot{q}$ is injected into adipose tissue. Assume that a fluid-filled reservoir of radius r_D and pressure p_D is formed at the tip of the needle, and the surrounding solid is of permeability k (see Figure 10). The volumetric flow rate $\dot{q}$ is related to the flow per unit area $\dot{u}(r)$ according to

$$\dot{u}(r) = \frac{\dot{q}}{4\pi r^2} \tag{7}$$

Substitution of (7) into (6) gives

$$-k\frac{\partial p}{\partial r} = \frac{\dot{q}}{4\pi r^2} \tag{8}$$
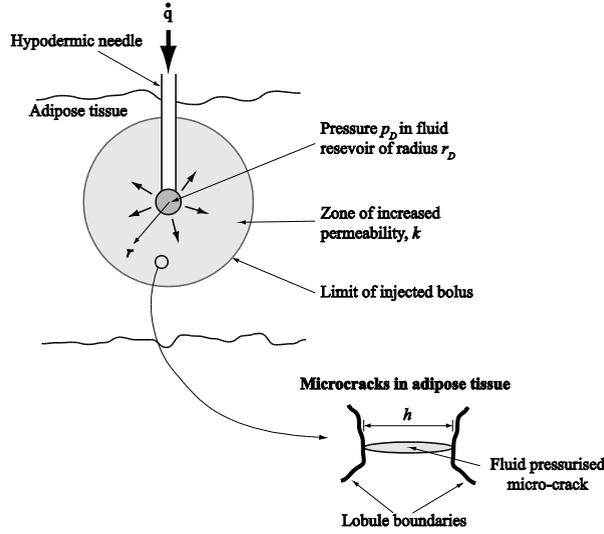
Figure 10. A sketch of the injection of a liquid into adipose tissue.

and thereby leads to an injection p_D at $r = r_D$ of

$$p_D = \frac{\dot{q}}{4\pi k r_D} \tag{9}$$

In order to perform an order of magnitude calculation for the permeability k it is assumed that $2r_D = 800\,\mu$m. This value matches the width of the fluid-filled channels observed in the x-ray images of Figure 9. Upon matching the regression coefficient $c = 740\,$GPa s m^{-3} of (5) to the constant of proportionality in (9) one obtains

$$c = \left(4\pi k r_D\right)^{-1} \tag{10}$$

and consequently $k = 2.7 \times 10^{-10}\,$m^4 N^{-1} s^{-1}.

How does this value compare with data reported in the literature? The permeability of adipose tissue for quasi-static flow is reported elsewhere to be between 1.8×10^{-12} and $1 \times 10^{-13}\,$m^4 N^{-1}s^{-1} [Guyton et al. 1966; Reddy et al. 1981]. These values are 10^2 and 10^3 times smaller than the permeability observed during the current injection tests. This indicates that injection of a pressurised fluid increases the permeability of the tissue by the creation of a connecting network of micro-cracks as observed in Figure 9. This phenomenon is analogous to hydraulic fracture of rocks where pumped fluid leads to the formation of a connecting network of cracks [Wang 2000].

Hydraulic fracture model. It is suggested that during injection the fluid tunnels through pathways of low resistance, possibly between lobules of adipocytes The mode I toughness J_C associated with the tunnelling fracture of a micro-crack of width h (see Figure 10), within a tissue of Young's modulus E and under a pressure p_0 is given in [Hutchinson and Suo 1991] as

$$J_C = \frac{p_0^2 h}{1.27E} \tag{11}$$

A measure of the pressure required to generate micro-cracks within the tissue is given by the value of $p_0 = 23$ kPa, taken from the least squares regression fit of the pressure data; see (5). Let the Young's modulus of adipose tissue be equal to $E = 1$ kPa [Comley and Fleck 2009]. Then for a crack of width $h = 800\,\mu$m (matching the width of the observed micro-cracks in Figure 9) the corresponding fracture toughness is of the order $J_C = 330$ Jm^{-2}. This is an order of magnitude lower than the fracture toughness of adipose tissue $J_C = 4.1$ kJ m^{-2}, as measured via trouser tear test [Comley and Fleck 2010b]. This result indicates that the pressurised fluid seeks out relatively brittle interfaces within the adipose tissue. Further work is required to examine the injection site within the tissue via microscopy, in order to confirm (or refute) our conjecture of hydraulic fracture along weak paths.

6. Concluding remarks

Measurements have been made of the pressure to penetrate adipose tissue by a solid punch and the pressure to inject adipose tissue with a low viscosity liquid. The punch pressure is about three orders of magnitude greater than the injection pressure, indicating that different fracture mechanisms are involved. It is shown that the deep penetration pressure can be adequately modelled by the Shergold-Fleck model for ring-cracks. A seepage model based on Darcy flow is presented to account for the linear dependence of delivery pressure on volumetric flow rate. The seepage model reveals that the permeability of the tissue is significantly increased during the injection event. X-ray images of the injected bolus within the tissue indicate the presence of micro-cracks, formed during injection. A hydraulic fracture model reveals a low value of toughness, $J_C = 330$ J m^{-2} associated with the formation of these micro-cracks.

Acknowledgements

References

[Barry et al. 1995] S. I. Barry, G. K. Aldis, and G. N. Mercer, "Injection of fluid into a layer of deformable porous medium", *Appl. Mech. Rev. (ASME)* **48**:10 (1995), 722–726.

[Baxter and Mitragotri 2005] J. Baxter and S. Mitragotri, "Jet-induced skin puncture and its impact on needle-free jet injections: experimental studies and a predictive model", *J. Control. Release* **106**:3 (2005), 361–373.

[Björntorp and Martinsson 1966] P. Björntorp and A. Martinsson, "The composition of human subcutaneous adipose tissue in relation to its morphology", *Acta Med. Scand.* **179**:4 (1966), 475–481.

[Comley and Fleck 2009] K. S. C. Comley and N. A. Fleck, "The high strain rate response of adipose tissue", pp. 27–33 in *IUTAM Symposium on Mechanical Properties of Cellular Materials* (Cachan, 2007), edited by H. Zhao and N. A. Fleck, IUTAM Bookseries **12**, Springer, Dordrecht, 2009.

[Comley and Fleck 2010a] K. S. C. Comley and N. A. Fleck, "A micromechanical model for the Young's modulus of adipose tissue", *Int. J. Solids Struct.* **47**:21 (2010), 2982–2990.

[Comley and Fleck 2010b] K. S. C. Comley and N. A. Fleck, "The toughness of adipose tissue: measurements and physical basis", *J. Biomech.* **43**:9 (2010), 1823–1826.

[Comley and Fleck 2011] K. S. C. Comley and N. A. Fleck, "The constitutive response of porcine adipose tissue", 2011. Submitted to *Int. J. Impact Eng.*

[Cooke et al. 1980] E. D. Cooke, S. A. Bowcock, A. Johnston, and A. T. Elliott, "Gas-powered jet injection compared with conventional methods of injection using lignocaine and technetium-99m", *Br. Med. J.* **281**:6241 (1980), 643–644.

[Gefen and Haberman 2007] A. Gefen and E. Haberman, "Viscoelastic properties of ovine adipose tissue covering the gluteus muscles", *J. Biomech. Eng. (ASME)* **129**:6 (2007), 924–930.

[Greenwood and Johnson 1983] M. R. C. Greenwood and P. R. Johnson, "The adipose tissue", pp. 178–199 in *Histology: cell and tissue biology*, 5th ed., edited by L. Weiss, Elsevier, New York, 1983.

[Guyton et al. 1966] A. C. Guyton, K. Scheel, and D. Murphree, "Interstitial fluid pressure, 3: Its effect on resistance to tissue fluid mobility", *Circ. Res.* **19**:2 (1966), 412–419.

[Hutchinson and Suo 1991] J. W. Hutchinson and Z. Suo, "Mixed mode cracking in layered materials", *Adv. Appl. Mech.* **29** (1991), 63–191.

[Miller-Young et al. 2002] J. E. Miller-Young, N. A. Duncan, and G. Baroud, "Material properties of the human calcaneal fat pad in compression: experiment and theory", *J. Biomech.* **35**:12 (2002), 1523–1531.

[Nakajima et al. 1998] I. Nakajima, T. Yamaguchi, K. Ozutsumi, and H. Aso, "Adipose tissue extracellular matrix: newly organized by adipocytes during differentiation", *Differ.* **63**:4 (1998), 193–200.

[Nightingale et al. 2003] K. Nightingale, S. McAleavey, and G. Trahey, "Shear-wave generation using acoustic radiation force: *in vivo* and *ex vivo* results", *Ultrasound Med. Biol.* **29**:12 (2003), 1715–1723.

[Ogden 1972] R. W. Ogden, "Large deformation isotropic elasticity: on the correlation of theory and experiment for incompressible rubberlike solids", *Proc. R. Soc. Lond. A* **326**:1567 (1972), 565–584.

[Reddy et al. 1981] N. P. Reddy, G. V. B. Cochran, and T. A. Krouskop, "Interstitial fluid flow as a factor in decubitus ulcer formation", *J. Biomech.* **14**:12 (1981), 879–881.

[Samani et al. 2003] A. Samani, J. Bishop, C. Luginbuhl, and D. B. Plewes, "Measuring the elastic modulus of *ex vivo* small tissue samples", *Phys. Med. Biol.* **48**:14 (2003), 2183–2198.

[Schramm-Baxter and Mitragotri 2004] J. Schramm-Baxter and S. Mitragotri, "Needle-free jet injections: dependence of jet penetration and dispersion in the skin on jet power", *J. Control. Release* **97**:3 (2004), 527–535.

[Shergold and Fleck 2004] O. A. Shergold and N. A. Fleck, "Mechanisms of deep penetration of soft solids, with application to the injection and wounding of skin", *Proc. R. Soc. Lond. A* **460** (2004), 3037–3058.

[Shergold and Fleck 2005] O. A. Shergold and N. A. Fleck, "Experimental investigation into the deep penetration of soft solids by sharp and blunt punches, with application to the piercing of skin", *J. Biomech. Eng. (ASME)* **127**:5 (2005), 838–848.

[Shergold et al. 2006] O. A. Shergold, N. A. Fleck, and T. S. King, "The penetration of a soft solid by a liquid jet, with application to the administration of a needle-free injection", *J. Biomech.* **39**:14 (2006), 2593–2602.

[Wang 2000] H. F. Wang, *Theory of linear poroelasticity with applications to geomechanics and hydrogeology*, Princeton Univ. Press, Princeton, NJ, 2000.

KERSTYN COMLEY: `kerst22@gmail.com`
Cambridge University, Department of Engineering, Trumpington Road, Cambridge CB2 1PZ, United Kingdom

NORMAN FLECK: `naf1@cam.ac.uk`
Cambridge University, Department of Engineering, Trumpington Road, Cambridge CB2 1PZ, United Kingdom